JOURNAL OF SOLID STATE CHEMISTRY 41, 174–184 (1982)

Structural Aspects and Magnetic Properties of the Lamellar Compound $Cu_{0.50}Cr_{0.50}PS_3$

P. COLOMBET, A. LEBLANC, M. DANOT, AND J. ROUXEL

Laboratoire de Chimie des Solides, L.A. 279, 2, rue de la Houssinière, 44072 Nantes Cedex, France

Received June 10, 1981; in revised form October 8, 1981

$Cu_{0.50}Cr_{0.50}PS_3$ is a new lamellar compound obtained from the elements at 700°C in evacuated silica tubes. The unit cell is monoclinic with $a = 5.916$ (1) Å; $b = 10.246$ (2) Å; $c = 13.415$ (5) Å; $\beta = 107.09$ (3)°. The structure is built up with $S|Cu_{0.33}Cr_{0.33}(P_2)_{0.33}|S$ slabs in which copper, chromium, and (P_2) pairs share the octahedral voids between two sulfur layers. Copper is not located at the center of its octahedral sites but is distributed among a continuous series of positions within these sites. This complex distribution has been simulated, attributing to copper two crystallographic eightfold positions with important thermal factors, especially perpendicular to the a–b plane. EPR studies and optical and magnetic measurements show that chromium is present as Cr^{3+} ions. The magnetic study suggests that, below $T_N \sim 30$ K, this compound is a weakly anisotropic antiferromagnet consisting possibly of ferromagnetic layers which are antiferromagnetically coupled to adjacent layers. A good fit with the experimental results is obtained by means of calculations performed on the basis of a two-dimensional Heisenberg model.

1. Introduction

The MPS_3 phases, where M is a bivalent metal, have been prepared by Hahn and Klingen (*1*) and Nitsche and Wild (*2*).

Klingen (*3*) has described the structure of $FePS_3$. He writes the formula as $Fe_2P_2S_6$ to show the occurrence of (P_2) pairs. This formula may also be written as $[Fe_{2/3}(P_2)_{1/3}]S_2$ in order to establish the relation with the MX_2 lamellar types. Actually, $FePS_3$ is a lamellar compound which can behave as a host structure in intercalation reactions (*4*), due to the presence of a Van der Waals gap between the slabs. The sulfur sequence is of the *ABC* type (and not *AB*, as in TiS_2), a slight distortion leading to a monoclinic symmetry. Iron and (P–P) pairs occupy ordered positions in the slabs and from one slab to another.

This structural type also occurs when replacing one Fe^{II} by ($\frac{2}{3}\,In^{III} + \frac{1}{3}\,\square$). It leads to $In_{2/3}\square_{1/3}PS_3$ (*5*), which can be related to the $CrCl_3$ type. The ability of this structural type to accept such a substitution suggests the possibility of replacing M^{II} by a couple ($0.5\,M^{I} + 0.5\,M^{III}$). The present work deals with the $Cu_{0.50}Cr_{0.50}PS_3$ compound. Chromium has been chosen because of the particular stability of its +3 oxidation state and on account of its pronounced preference for octahedral sites.

2. Experimental

2.1. Synthesis of $Cu_{0.50}Cr_{0.50}PS_3$ and Chemical Analysis

As reported in a previous short note (*6*), $Cu_{0.50}Cr_{0.50}PS_3$ has been prepared from the

0022-4596/82/020174-11$02.00/0

elements, at 700°C, in evacuated silica tubes. The formula was checked by chemical analysis for powders and by a microprobe technique for crystals (*6*).

2.2. X-Ray Study

A single crystal study showed the symmetry to be monoclinic, space group *Cc* or *C2/c*. The cell parameters, least squares refined from powder spectra, are: $a = 5.916$ (1) Å, $b = 10.246$ (2) Å, $c = 13.415$ (5) Å, $\beta = 107.09$ (3)°.

The experimental density is in good agreement with the value calculated for $Z = 8$ ($d_{calcd} = 3.12$ for $d_{meas} = 3.08$).

The crystal chosen for the structural study was a 0.1-mm-thick prism, with an equilateral triangular base (side: 0.2 mm). The intensities of 1664 crystallographic independent reflections were measured, in the θ range 4–40°, with a CAD 3 Nonius automatic diffractometer according to the θ–2θ scan technique, with $\Delta\theta$ (°) = 1.1 + 0.4 tg θ, and using Mo$K\alpha$ radiation. The intensity data were converted into observed structure factors by applying the standard Lorentz and polarization corrections. The linear absorption coefficient is $\mu = 59.8$ cm^{-1}. Absorption corrections were computed with a program adapted from Data P1 (*7*); the transmission factors lay in the range 0.47–0.61.

2.3. NMR Analysis

NMR measurements were performed at 22 MHz and 300 K on ^{31}P using a SXP Brüker spectrometer (pulsed method). The spin lattice relaxation time was measured by observing magnetization recovery vs time in a $\Pi - \Pi/2$ pulse sequence.

2.4. Magnetic Measurements

From 4.2 to 300 K, susceptibility measurements were carried out on a Faraday balance system (resolution of 1μg). Several field strengths were used, ranging from 2.8 to 6.7 kG, platinum being the standard. The susceptibilities are given with an accuracy of about 10^{-2}. Both powder and crystal[1] were studied. The susceptibility of a single crystal placed in a silica bucket was determined with the applied field perpendicular, and then parallel, to c', c' being the axis perpendicular to the sulfur sheets.

Magnetization curves were obtained for powders at the Laboratoire Louis Neel in Grenoble, up to 60 kG using the extraction method.

2.5. EPR Spectra

EPR spectra of a crystal were recorded at 300 K on an X-band spectrometer. g factors were measured using diphenylpicrylhydrazine as an internal standard.[2]

2.6. Optical Spectrum Recording

Unfortunately, it was not possible to get the absorption spectrum of $Cu_{0.50}Cr_{0.50}PS_3$ because we could not obtain thin enough crystals. Thus we used diffuse reflectance technique. The spectrometer was a Unicam SP8-100, working from 300 to 800 nm.

3. The Structure of $Cu_{0.50}Cr_{0.50}PS_3$

3.1. Determination of the Structure

The cell parameters of $Cu_{0.50}Cr_{0.50}PS_3$ (a, b, c, β) are related to those of $FePS_3$ (a', b', c', β') by $a \simeq a'$, $b \simeq b'$, $c \simeq 2c'$, $\beta = \beta'$, but the reflections that imply doubling of c' are not systematically weak.

According to the c periodicity and following the chemical composition, chromium could occupy in an ordered way half of the iron sites, with an alternated stacking of these ordered a–b planes.

So, the first calculations were performed

[1] The crystal study was carried out with the apparatus of O. Gorochov, Laboratoire de Physique des Solides, CNRS – 92190 Meudon, France.

[2] EPR spectra were obtained at Laboratoire de P.M.C., Ecole Polytechnique, Palaiseau, France.

taking only into account phosphorus and chromium (according to an ordered distribution) and sulfur. The more symmetrical $C2/C$ space group was adopted for these calculations.

The atomic positions were chosen as follows:

—Sulfur in $8f$, with

$$x \simeq \tfrac{1}{4},\quad y \simeq \tfrac{1}{8},\quad z \simeq \tfrac{3}{8}\quad (A)$$

$$x \simeq \tfrac{1}{4},\quad y \simeq \tfrac{1}{8},\quad z \simeq \tfrac{7}{8}\quad (B)$$

$$x \simeq \tfrac{3}{4},\quad y \simeq 0,\quad z \simeq \tfrac{3}{8}\quad (C);$$

—Phosphorus in $8f$, with $x \simeq 0.06$, $y \simeq \frac{1}{3}$, $z \simeq 0.83$;

—Chromium in $4e$, with $x = 0$, $y \simeq \frac{1}{3}$, $z = \frac{1}{4}$.

After five cycles, these coordinates were refined to the values given in Table I, the R factor being equal to 0.187. A difference Fourier map (Fig. 1) shows, in the x–z plane, a long cloud perpendicular to the x axis, and located in every second iron octahedron of the $FePS_3$ model. So, one-half of these iron octahedra are occupied by chromium, the others by copper.

The electron density cloud exhibits three extrema. One of them is in the middle; the other two are sharper, higher, and located close to each extremity. But, according to the chemical composition, one of these octahedra is occupied by one copper only. So, in fact, the occurrence of such an electron density map reveals the possibility for copper to occupy, according to a given occupancy ratio, every position located in this

TABLE I

ATOMIC COORDINATES REFINED WITHOUT TAKING COPPER INTO ACCOUNT

	x	y	z	B
A Sulfur	0.2470	0.1821	0.3736	1.03
B Sulfur	0.2658	0.1708	0.8735	1.09
C Sulfur	0.7249	0.9963	0.3755	1.13
Phosphorus	0.0529	0.3329	0.8341	0.77
Chromium	0	0.3346	0.25	0.64

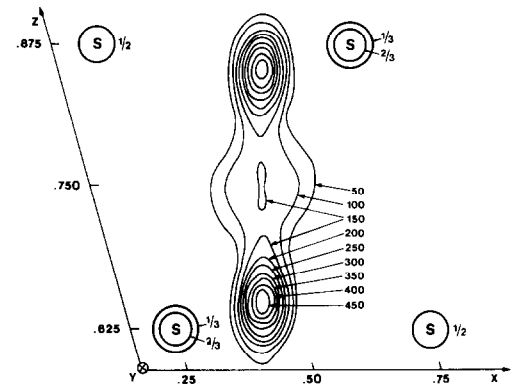

FIG. 1. Difference Fourier map ($y = 0.50$) showing the copper electron density in the sulfur octahedron. The scale factor for the electronic density is 28.1.

cloud, the extrema corresponding to more favorable positions. Such a distribution would allow copper to accommodate Cu–S distances comparable with those which commonly exist in $[CuS_4]$ tetrahedra. It is obvious that only a statistical picture of such a phenomenon can be given by X-ray. To simulate the copper distribution, we introduced in the calculations two eightfold positions. One of them corresponds to the maxima located near the upper and the lower triangle of the octahedron. The second one leads, in a given octahedron, to two equivalent positions in the vicinity of the octahedron center. The occupancy ratios were fixed, respectively, proportional to the estimated importance of the extrema (A copper, near the bases: $\tau = 0.33$; B copper, near the octahedron center: $\tau = 0.17$). After refinement, we obtained for copper the values given in Table II.

The R factor was 0.143. The appreciable B factors are not surprising since we tried

TABLE II

ATOMIC COORDINATES OF COPPER

	x	y	z	B
A copper	0.0613	0.0021	0.3492	3.55
B copper	0.5136	0.5024	0.2763	3.00

to describe a continuous phenomenon with a finite number of crystallographic positions. Upon introducing the U_{ij} anisotropic thermal factors, the R factor dropped to 0.056. This significant improvement is related to the fact that anisotropic factors give a much better picture of the copper distribution. In spite of this good final R value, we tried to refine the occupancy ratios, but, even after eight cycles, the copper parameters did not stabilize, due to important correlations. These correlations induce estimated standard deviations for copper that are larger than those for the other atoms (see Table III).

However, in spite of these correlations, the sum of the occupancy ratios always remained equal to the effective copper amount, within the experimental uncertainty. The R factor was not affected, even for τ values quite different from 0.33 and 0.17, because atomic coordinates and U_{ij} were then refined to come to an agreement with the τ values.

Table III gives the final results of the structural study.

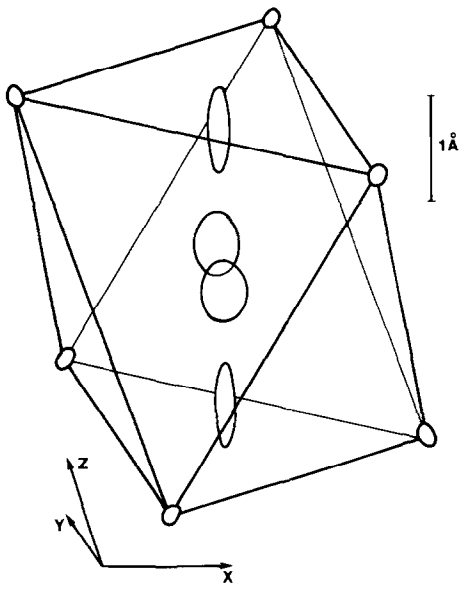

FIG. 2. Thermal vibrational ellipsoids of copper. The ellipsoids of sulfur are given for comparison.

TABLE III

FINAL RESULTS OF THE STRUCTURAL STUDY

Atom	x	y	z	U_{11}	U_{22}	U_{33}	U_{23}	U_{13}	U_{12}
A Sulfur	0.2471(2)	0.1823(1)	0.3736(1)	0.0085(3)	0.0149(4)	0.0168(4)	0.0062(3)	0.0067(3)	0.0041(3)
B Sulfur	0.2656(2)	0.1724(1)	0.8736(1)	0.0114(3)	0.0135(4)	0.0162(4)	0.0062(3)	0.0076(3)	0.0056(3)
C Sulfur	0.7240(2)	0.9956(1)	0.3757(1)	0.0092(3)	0.0094(4)	0.0176(4)	−0.0011(3)	−0.0027(3)	0.0022(3)
Phosphorus	0.0533(2)	0.3319(1)	0.8344(1)	0.0061(3)	0.0093(4)	0.0109(4)	−0.0002(3)	0.0021(3)	−0.0002(3)
Chromium	0	0.3351(1)	0.25	0.0053(3)	0.0082(4)	0.0108(3)	0.0015(16)	0.0022(2)	−0.0054(13)
A Copper	0.0607(5)	0.0021(3)	0.3482(5)	0.0241(11)	0.0127(10)	0.1709(46)	−0.0006(21)	0.0510(20)	0.0000(9)
B Copper	0.4966(37)	0.5020(9)	0.2670(14)	0.0448(33)	0.0503(37)	0.0888(123)	−0.0022(58)	0.0384(75)	0.0007(47)

The U_{ij} values behave differently for the two copper positions: for the *A* position, the thermal ellipsoid is very elongated perpendicular to the *a–b* plane (Fig. 2). For the *B* position, the U_{ij} values are large too, but the ellipsoid does not differ a lot from a sphere (Fig. 2). These ellipsoids are connected to the distribution of copper within the sulfur octahedron. Appreciable thermal factors have already been observed for copper, which has been found to be distributed around the center of its site (*8–10*).

As the *Cc* space group had no reason to be excluded, we tried some calculations in this noncentrosymmetric group. Instead of the considerably larger variable number, the *R* factor was not significantly better. So the right space group is actually *C*2/*c*.

3.2. Description of the Structure, Comparison with $FePS_3$

The structure of $Cu_{0.50}Cr_{0.50}PS_3$ derives from that of $FePS_3$: it is a layered structure built on an *ABC* sulfur stacking. The Van der Waals gap is completely empty. The octahedral sites of the so-called "filled layer" are occupied, in an ordered way (Fig. 3), by chromium for one-third of these sites, by phosphorus pairs for the second third, and, by copper for the last third. The positions and U_{ij} we refined for copper are only a poor representation of the actual phenomenon, which is better described by the difference Fourier map (Fig. 1). On this map, the density calculated for any point is related to the copper presence probability at this point.

All the octahedra are distorted, as shown in Fig. 4. The interatomic distances observed for $FePS_3$ (*3*) are given, to allow a comparison. In $FePS_3$, the P_2-containing and the Fe-containing octahedra are almost the same size. If we now consider $Cu_{0.50}Cr_{0.50}PS_3$, the P_2-containing octahedra do not change a lot, but their distortion increases. The $[CrS_6]$ octahedra are smaller, and the $[CuS_6]$ ones larger than the

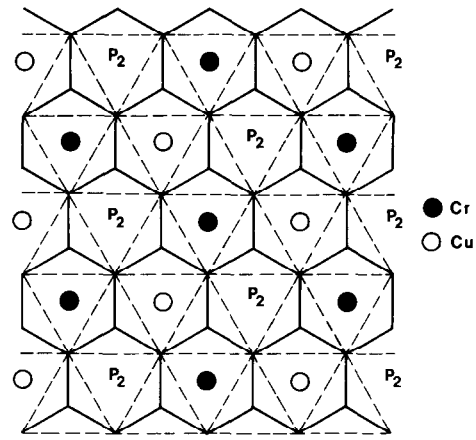

FIG. 3. Ordered distribution of Cr, Cu, and P_2 pairs in the *a–b* plane.

$[FeS_6]$ octahedra. Both Cr- and Cu-containing octahedra are more distorted than the $[FeS_6]$ ones.

Table IV gives the cation–sulfur distances. The Cr–S distances are quite consistent with what can be expected. Tretyakov *et al.* (*11*), for instance, tabulated a typical $d(Cr^{III}–S)$ equal to 2.41 Å. The P–S bond length perfectly agrees with the value calculated for $FePS_3$ (2.030(6) Å). The Cu–S distances have not to be taken for absolute values, as we showed when discussing the copper atomic parameters refinement. The *A* copper positions are close to the upper and to the lower triangles of the octahedron. Even for the *B* sites copper comes close to sulfur triangles (lateral ones) as shown by the occurrence of three shorter

TABLE IV

CATION–SULFUR DISTANCES

	A Sulfur	*B* Sulfur	*C* Sulfur
Chromium	2.432(1)	2.456(1)	2.448(1)
Phosphorus	2.034(1)	2.034(1)	2.030(1)
	3.337(1)	3.305(1)	3.323(1)
A Copper	2.126(3)	2.131(3)	2.131(3)
	3.520(3)	3.521(3)	3.591(3)
B Copper	2.532(9)	2.537(9)	2.474(9)
	2.729(9)	2.727(9)	2.873(9)

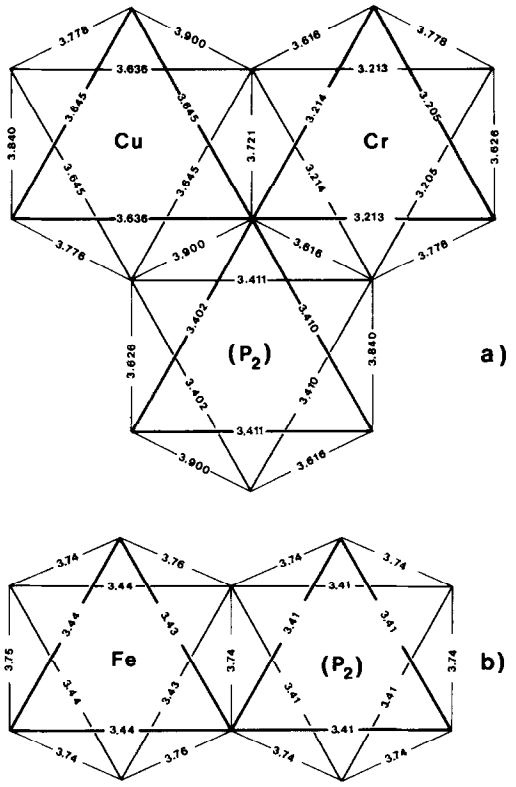

FIG. 4. Different octahedra occurring in the structures of $Cu_{0.50}Cr_{0.50}PS_3$ (a) and of $FePS_3$ (b).

and three longer Cu–S bonds. The P–P distance is 2.165(2) Å, which compares well with 2.190(8) Å calculated by Klingen (*3*) for $FePS_3$.

4. Physical Properties of $Cu_{0.50}Cr_{0.50}PS_3$: A Magnetic Model

4.1. Physical Properties

The ^{31}P resonance line at room temperature has a width at half-height equal to 4.5 G and a shift equal to -3.3×10^{-3}, H_3PO_4 being taken as the reference. The spin relaxation time T_1 is equal to 0.65 msec, which is intermediate between those observed in $FePS_3$ and $NiPS_3$ (*12*). The resonance linewidth alone cannot be taken as a proof of the occurrence of the phosphorus pairs and the corresponding small P–P distance determined by X-ray analysis (2.165 Å). Indeed, our measurements were performed on a powder sample, and it is not possible to separate the effect of dipolar coupling between ^{31}P nuclear spins and their coupling with the electronic spins of the paramagnetic Cr^{3+} (*13*).

Above 60 K the magnetic susceptibility corrected for diamagnetism contribution obeys the Curie–Weiss law $\chi = C/(T - \theta_p)$, where C and θ_p are the Curie and Weiss constants, respectively. The effective moment (4.08 μ_B) is very close to the spin-only value for a Cr^{3+} ion. θ_p is positive ($\simeq$ 31.5 K). Yet, as illustrated in Fig. 5a, a sharp maximum is observed, indicating an antiferromagnetic spin arrangement at low temperature. The magnetic parameters are summarized in Table V. Figure 5b shows a plot of χ versus temperature for a single crystal with the c' axis perpendicular, and then parallel, to H. The positions of the maxima in the susceptibility (T_{max}) for both directions are the same as for the powder (31.5 K). At 4.2 K, $\chi_\perp$ and $\chi_\parallel$ differ by only 10%, which is far from what we could expect for a normal antiferromagnet.

$Cu_{0.50}Cr_{0.50}PS_3$ is dark brown. The diffuse reflectance spectra are poorly resolved. Nevertheless, in the range 13,000 to 16,000 cm^{-1}, a minimum is observed which may be attributed to the first allowed transition $^4A_2$

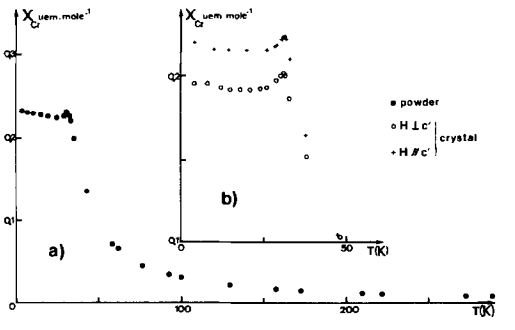

FIG. 5. Temperature dependence of χ, for a powder sample (a), and for a single crystal (b).

TABLE V

PARAMETERS RELATED TO THE MAGNETIC BEHAVIOR OF $Cu_{0.50}Cr_{0.50}PS_3$

C	μ_{eff} (μ_B)	θ_P (K)	T_{max} (K)	$g_\perp$	$g_\parallel$	10 Dq (cm^{-1})	k
2.08	4.08	31.5	31.5	1.991	1.988	14500	0.5

$\rightarrow {}^4T_2$ expected for chromium d^3 in an octahedral environment. We did not observe either the other d–d transitions (${}^4A_2 \rightarrow {}^4T_1$ (F); ${}^4A_2 \rightarrow {}^4T_1$ (P)) or the fundamental charge transfer. The large width of the transition ($\simeq$ 3000 cm^{-1}) is probably due to the splitting of the excited state by the distortion of the octahedral site of chromium. Such a wide transition has already been observed in $CrPS_4$ (*14*).

EPR spectra were obtained on a single crystal in two directions, with H perpendicular to c', and then parallel to c'. We obtained $g_\perp = 1.991$ and $g_\parallel = 1.988$ in good agreement with the presence of d^3 chromium with a ${}^4A_2$ ground term.

Due to second-order effects of the component of the ${}^4T_2$ term on the ${}^4A_2$ term, the molar susceptibility may be expressed (*15*) as

$$\chi_{mol}^{obsd} = \chi_{mol}^{S}\left(1 - \frac{4k^2\lambda}{10\,Dq}\right)^2 + \frac{8Nk^2\mu_B^2}{10\,Dq}, \quad (1)$$

where $\chi_{mol}^{S} = Ng^2\mu_B^2 S(S+1)/3kT$ is the spin-only contribution to the susceptibility, μ_B is the Bohr magneton, λ the spin-orbit coupling constant in the free Cr^{3+} ion, 10 Dq the crystal field parameter, and k the orbital reduction factor. With $g = 1.990$ for powders and $10\,Dq = 14{,}500$ cm^{-1} (which is approximately the middle of the observed transition), a k value of 0.5 is obtained. Compared to the results reported for $A\,CrO_2$ (A = Li, Na, K) (*16*) the smaller value for k is related to the more covalent character of the Cr–S bond. The spin-only contribution χ_{mol}^{S} calculated from Eq. (1) is plotted versus T in Fig. 6. The temperature-independent term in Eq. (1) is equal to 35×10^{-6} emu · mole^{-1}. We did not take any Pauli paramagnetism into consideration because of the very high resistivity of $Cu_{0.50}Cr_{0.50}PS_3$. Indeed, an attempt to measure the resistivity of a single crystal failed, its resistance being higher than 10^{12} ohms, which was the limit of our apparatus.

4.2. Field Dependence of Powder Susceptibility of $Cu_{0.50}Cr_{0.50}PS_3$ below 35 K

Susceptibility begins to depend significantly on the applied field only when we reach the temperature at which we noticed the cusp. From $\simeq$35 to $\simeq$30 K the variation is weak and linear and becomes more important below 31.5 K (Fig. 7a). For $T < 30$ K the variation increases and is no longer linear. The accuracy of the measurements for fields lower than 2.5 kG is not sufficient to allow a determination, by extrapolation, of the zero-field susceptibility

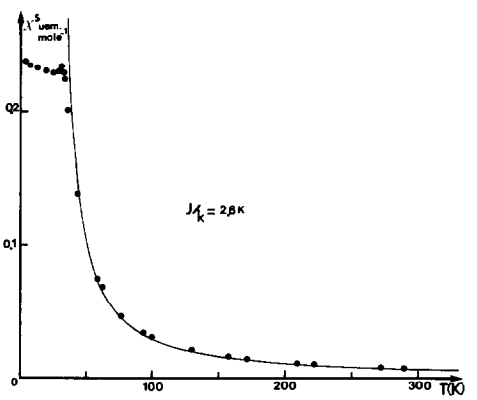

FIG. 6. Fitting of the experimental $\chi^S = f(T)$ curve. The experimental points are shown by ●, and the theoretical curve is the continuous line.

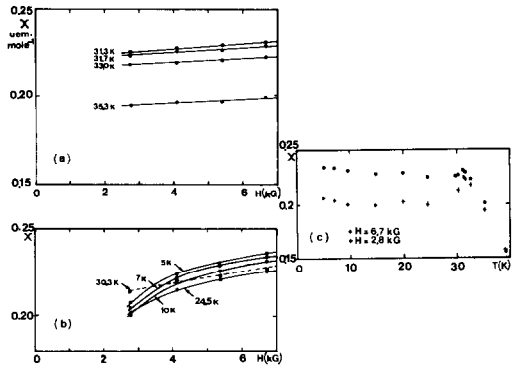

FIG. 7. Field dependence of the susceptibility (a) above and (b) below 31 K. Temperature dependence of χ for two values of the applied field (c).

of $Cu_{0.50}Cr_{0.50}PS_3$. A survey of Fig. 7b, which shows a plot of χ vs H, suggests, nevertheless, that below the cusp the zero-field susceptibility has a value far lower than what we plotted in Fig. 5, which corresponds to $H = 6.7$ kG. Thus the zero-field susceptibility of a powder over the region from 4.2 to 31.5 K might be what we could expect for a normal antiferromagnet, i.e., decreasing χ with decreasing temperature. Figure 7c shows the experimental susceptibility for the lowest and highest values of the external field we used.

Such a field dependence could be due to a ferromagnetic impurity. So, it cannot be related to the presence of $CrPS_4$, the most probable impurity, which is antiferromagnetic (*14*). Further, χ depends on the applied field below 35 K (near T_{max}) and it is hardly to be expected that a ferromagnetic impurity could produce this dependence only in the temperature region from 4.2 to 35 K. Moreover, the χ values have been found to be identical for various samples obtained from different preparations. All these considerations exclude the effect of impurities.

4.3. A Magnetic Model for $Cu_{0.50}Cr_{0.50}PS_3$

The positive value of the paramagnetic Curie temperature suggests that the predominant magnetic interactions are ferromagnetic. Yet, there is a cusp in the susceptibility.

A positive value of θ_p does not preclude an antiferromagnetic ordering at low temperature: in some layered ternary chalcogenides, such as $NaCrS_2$, $KCrS_2$, $NaCrSe_2$, and $AgCrSe_2$, similar magnetic curves have been observed, the *AF* spin arrangement being confirmed by neutron diffraction (*17–19*). The predominant positive intralayer interactions ($J_{intra} > 0$) are responsible for the positive θ_p, but the adjacent layers are antiferromagnetically coupled at low temperature ($J_{inter} < 0$). The magnetic behavior of $Cu_{0.50}Cr_{0.50}PS_3$ is probably the same as that of the M^ICrX_2 compounds mentioned above.

The choice of a similar two-dimensional magnetic model for $Cu_{0.50}Cr_{0.50}PS_3$ is justified by two facts: (i) the distance between nearest neighbor magnetic ions (Cr) within the layer is shorter than between two neighboring layers (5.92 and 6.72 Å, respectively), and (ii) the number of intralayer nearest neighbors is larger than the interlayer number ($z_{intra} = 6$ and $z_{inter} = 2$). Figure 8 shows the plane triangular chromium lattice in the *a–b* layer.

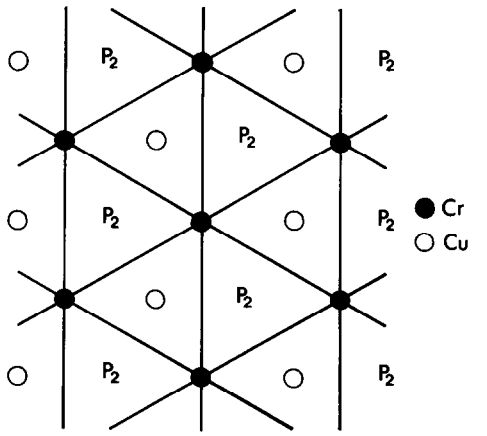

FIG. 8. Triangular planar lattice of chromium in the *a–b* plane.

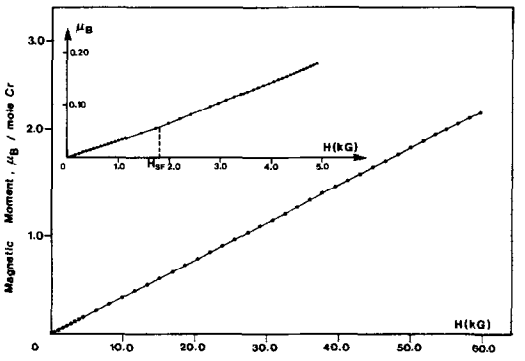

FIG. 9. Molar magnetization at 4.2 K as a function of applied field, for a powder sample.

In order to explain the field dependence of the susceptibility associated to the ordered state, magnetization measurements were performed on powder from 4.2 to 50 K. They confirm the antiferromagnetic ordering at low temperature with $T_N \sim 30$ K: neither remanent magnetization nor coercive field were observed. The variation of the magnetization as a function of field at 4.2 K is sketched in Fig. 9. The discontinuity at $H \sim 1.8$ kG probably indicates a spin–flop transition (*20, 21*). Consequently, in the external field range we used for susceptibility measurements (2.8 to 6.7 kG), the spins have already flipped over to the perpendicular orientation, leading to $\chi_{\parallel} \sim \chi_{\perp}$. Furthermore, the variation of χ (defined as σ/H) with the applied field H (Fig. 7) is related to this transition.

The low value of H_{SF} (1.8 kG) shows that $Cu_{0.50}Cr_{0.50}PS_3$ is a weakly anisotropic antiferromagnet, which is not surprising, Cr^{3+} being in a $^4A_2$ ground term.

4.4. Exchange Interactions and Geometric Aspects

The magnetic interactions of $Cu_{0.50}Cr_{0.50}PS_3$ are described by the Heisenberg model. Rushbrooke and Wood (*22*) have determined the first six coefficients in the expansion of the susceptibility in ascending powers of the reciprocal temperature. They consider only nearest-neighbor interacting ions.

If we assume that the planar ferromagnetic interactions are predominant in the high-temperature region, the relationship giving the temperature dependence of the reciprocal molar susceptibility is

$$(\chi^S)^{-1} = \frac{3\,kT}{Ng^2\mu_B^2 S(S+1)} [1 - 15x + 45x^2 + 148.5x^3 + 15.625x^4 - 2557.775x^5 - 11095.79x^6 + \ldots], \quad (2)$$

where $x = J/kT$ is positive, and $(\chi^S)^{-1}$ is the spin-only value which corresponds to Eq. (1). Equation (2) is obtained for a planar triangular lattice ($z = 6$). The best curve fitting, obtained for $J/k = 2.6$ K, is shown in Fig. 6. The agreement between χ^S_{calcd} and χ^S_{obsd} is good down to 40 K. The R factor, defined as $\Sigma (\chi_{obsd} - \chi_{calcd})^2/\Sigma \chi_{obsd}^2$, is then equal to 6×10^{-3} in the region from 40 to 300 K. The discrepancy at lower temperature appears when interplanar antiferromagnetic interactions become important, corresponding to a three-dimensional magnetic phase.

As for the interplanar exchange energy, a rough estimation of its value is given within the molecular field theory (*23*) by the relation

$$(\chi^S)^{-1}(T_{max})\,C_M = \tfrac{8}{3}\frac{|J|}{k} S(S+1),$$

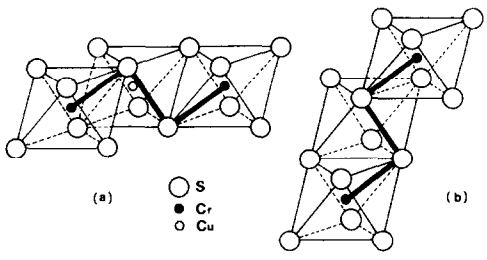

FIG. 10. Intralayer (a) and interlayer (b) possible superexchange pathways between two neighboring chromium.

TABLE VI

GEOMETRIC PARAMETERS OF THE SUPEREXCHANGE PATHWAY Cr–S–S–Cr BETWEEN TWO NEAREST NEIGHBORING CHROMIUM (θ IS THE CrSS OR SSCr ANGLE)

	θ (degrees)	d_{Cr-Cr} (Å)	J/k (K)
Intralayer	83.7 84.1 84.3	5.92	+2.6
Interlayer	103.2	6.72	−1

where $C_M = Ng^2\mu_B^2 S(S+1)/3k$. This relation is established for $z = 2$. J_{inter}/k is found to be equal to -1 K. J_{intra} and $|J_{inter}|$ are of the same order of magnitude. This is not surprising since $d_{inter}/d_{intra} = 1.13$. Thus $Cu_{0.50}Cr_{0.50}PS_3$ is not a so-called two-dimensional magnet in the whole explored temperature range, but such a procedure explains quite well the experimental results and the easy shift of dimensionality for the magnetic system.

For both intralayer and interlayer interactions, the large distance between the magnetic ions (5.92 and 6.72 Å) makes direct exchange extremely unlikely. The shortest superexchange pathway involves two sulfur atoms and is the same for both interlayer and intralayer interacting ions, as shown in Fig. 10. However, the geometric parameters for these entities differ slightly. They are given in Table VI.

It is known that a variation of the geometrical configuration of the cation–anion–cation complex taken as the basic unit in evaluating the magnetic interactions may influence dramatically the exchange constant J/k (see, for example, (*24*)), even for very small variations (*25*). Indeed, in $Cu_{0.50}Cr_{0.50}PS_3$, when d_{Cr-Cr} increases (the CrSS and SSCr angles increase simultaneously), the interaction is found to change in sign. However, the superexchange interactions are long range and probably do not involve only Cr–S–S–Cr pathways. The magnetic $3d^3$ chromium may interact via Cr–S–Cu–S–Cr within the layer, whereas it is impossible between following layers due to the Van der Waals vacancies. This also could explain why interlayer and intralayer interactions are of opposite sign as we assume in order to explain the whole magnetic behavior of $Cu_{0.50}Cr_{0.50}PS_3$.

Acknowledgments

The authors are indebted to Dr. G. Le Flem, Laboratoire de Chimie du Solide de Bordeaux I, Talence, for critical reading of the present paper. Thanks are due to Dr. Feron for helpful discussions and to Mr. A. Barlet and P. Le Thullier from Louis Neel Laboratory in Grenoble for collaboration in carrying out the magnetization measurements.

References

1. H. HAHN AND W. KLINGEN, *Natürwissen* **52,** 494 (1965).
2. R. NITSCHE AND P. WILD, *Mater. Res. Bull.* **5,** 419 (1970).
3. W. KLINGEN, Dissertation, University of Hohenheim (1969).
4. R. BREC, D. M. SCHLEICH, G. OUVRARD, A. LOUISY, AND J. ROUXEL, *Inorg. Chem.* **18,** 114 (1979).
5. S. SOLED AND A. WOLD, *Mater. Res. Bull.* **11,** 657 (1976).
6. A. LEBLANC AND J. ROUXEL, *C. R. Acad. Sci. Paris C* **291,** 12, 263 (1980).
7. B. G. BRANDT AND A. G. NORD, "Data P1, An Absorption Correction Program." Institute of Inorganic and Physical Chemistry, Stockholm (1970).
8. N. LE NAGARD, G. COLLIN, AND O. GOROCHOV, *Mater. Res. Bull.* **12,** 975 (1977).
9. N. LE NAGARD, O. GOROCHOV, AND G. COLLIN, *Mater. Res. Bull.* **10,** 1287 (1975).
10. N. LE NAGARD, Thèse d'Etat, p. 89, Orsay (1976).
11. YU. D. TRETYAKOV, I. V. GORDEEV, AND YA. A. KESLER, *J. Solid State Chem.* **20,** 345 (1977).
12. C. BERTHIER, Y. CHABRE, AND M. MINIER, *Solid State Commun.* **28,** 327 (1978).
13. G. OUVRARD, Thèse d'Etat, University of Nantes (1980).
14. A. LOUISY, G. OUVRARD, D. M. SCHLEICH, AND R. BREC, *Solid State Commun.* **28,** 61 (1978).

15. F. E. MABBS AND D. J. MACHIN, *in* "Magnetism and Transition Metal Complexes," pp. 14–22, Chapman & Hall, London (1973).
16. G. LE FLEM, C. DELMAS, F. MENIL, M. NIEL, C. CROS, C. FOUASSIER, AND M. POUCHARD, *J. Phys. (Orsay, Fr.)* **38,** C7–C262 (1977).
17. P. F. BONGERS, C. F. VAN BRUGGEN, J. KOOPSTRA, W. P. F. A. M. OMLOO, G. A. WIEGERS, AND F. JELLINEK, *J. Phys. Chem. Solids* **29,** 977 (1968).
18. B. VAN LAAR AND F. M. R. ENGELSMAN, *J. Solid State Chem.* **6,** 384 (1973).
19. F. M. R. ENGELSMAN, G. A. WIEGERS, F. JELLINEK, AND B. VAN LAAR, *J. Solid State Chem.* **6,** 574 (1973).
20. R. L. CARLIN AND A. J. VAN DUYNEVELDT, *in* "Magnetic Properties of Transition Metal Compounds," p. 172, Springer-Verlag, New York (1977).
21. A. HERPIN, *in* "Théorie du Magnétisme," p. 477, Bibliothèque des Sciences et Techniques Nucléaires, P.U.F. (1968).
22. G. S. RUSHBROOKE AND P. J. WOOD, *Mol. Phys.* **1,** 257, (1958).
23. D. H. MARTIN, *in* "Magnetism in Solids," p. 273, Iliffe, London (1967).
24. L. J. DE JONGH AND R. BLOCK, *Physica B + C (Amsterdam)* **79,** 568 (1975).
25. O. KAHN AND M. F. CHARLOT, *Nouv. J. Chim.* **4,** 567 (1980).